Low-Resolution Structures of Thyroid Hormone Receptor Dimers and Tetramers in Solution†

Ana Carolina Migliorini Figueira,‡ Mario de Oliveira Neto,‡ Amanda Bernardes,‡ Sandra Martha Gomes Dias,§ Aldo F. Craievich,|| John D. Baxter,⊥ Paul Webb,⊥ and Igor Polikarpov*,‡

Instituto de Física de São Carlos, Universidade de São Paulo, Av. Trabalhador Sãocarlense, 400, São Carlos, SP, Brazil 13560-970, Molecular Medicine Department, College of Veterinary Medicine, Cornell University, Ithaca, New York 14853, Instituto de Física, Universidade de São Paulo, São Paulo, SP, Brazil, and Metabolic Research Unit, Diabetes Center, and Department of Medicine, University of California, San Francisco, California 94143

Received August 19, 2006; Revised Manuscript Received November 25, 2006

ABSTRACT: High-resolution X-ray structures of thyroid hormone (TH) receptor (TR) DNA and ligand binding domains (DBD and LBD) have yielded significant insights into TR action. Nevertheless, the TR DBD and LBD act in concert to mediate TH effects upon gene expression, and TRs form multiple oligomers; however, structures of full-length TRs or DBD−LBD constructs that would clarify these influences are not available. Here, we report low-resolution X-ray structures of the TRβ DBD−LBD construct in solution which define the shape of dimers and tetramers and likely positions of the DBDs and LBDs. The holo TRβ DBD−LBD construct forms a homodimer with LBD−DBD pairs in close contact and DBDs protruding from the base in the same direction. The DBDs are connected to the LBDs by crossed extended D domains. The apo hTRβ DBD−LBD construct forms tetramers that resemble bulged cylinders with pairs of LBD dimers in a head-to-head arrangement with DBD pairs packed tightly against the LBD core. Overall, there are similarities with our previous low-resolution structures of retinoid X receptors, but TRs exhibit two unique features. First, TR DBDs are closely juxtaposed in the dimer and tetramer forms. Second, TR DBDs are closely packed against LBDs in the tetramer, but not the dimer. These findings suggest that TRs may be able to engage in hitherto unknown interdomain interactions and that the D domain must rearrange in different oligomeric forms. Finally, the data corroborate our suggestion that apo TRs form tetramers in solution which dissociate into dimers upon hormone binding.

Thyroid hormone (TH)[1] is critical for differentiation, growth, and metabolism and is a major regulator of mitochondrial activity (*1*−*4*). TH, in the form of triiodothyronine (T_3), exerts most of its effects by binding to thyroid hormone receptors (TRs), which are members of the nuclear receptor (NR) family of transcription factors (*5*). To perform their actions, the TRs interact with thyroid hormone response elements (TREs) comprised of repeats of the half-site AGGTCA in target promoters and recruit coregulators required for basal and T_3-dependent gene transcription (*1*−*5*). An improved understanding of TR structure and function will help us to determine how TRs regulate gene expression, how TR signaling pathways become dysregulated in disease, and how one can selectively modulate TR actions to treat high cholesterol, obesity, and other conditions (*6*). In addition, there are strong similarities between structures and actions of TRs and other NRs, so an improved understanding of TR function will help to clarify the mechanism of action of the whole NR family (*1*, *5*).

TRs conform to the typical organization of the NRs (Figure 1A): an N-terminal region (A/B domain) that is poorly conserved throughout the family, a central well-conserved DNA binding domain (DBD, C domain), a nonconserved D domain or hinge, and a C-terminal, moderately conserved, ligand binding domain (LBD, E domain) (*5*). The DBD is composed of two zinc fingers that target the receptor to specific TREs and is also involved in heterodimerization with the closely related retinoid X receptor (RXR) (*7*). The carboxy-terminal ligand-binding domain (LBD) binds T_3, contains a surface involved in homo- and heterodimer formation, and mediates the effects of T_3 upon gene expression via hormone-dependent conformational changes that lead to dissociation of corepressors and association of coactivators (*1*, *5*, *8*−*12*).

† This work was supported by a grant from the Conselho Nacional de Desenvolvimento Científico e Tecnológico (CNPq) to I.P. (300220/96-0), by Fundação de Amparo à Pesquisa do Estado de São Paulo (FAPESP) Grants 03/09462-5, 02/14041-6, 99/03387-4, and 06/00182-8, by São Paulo University, and by grants from the National Institutes of Health to J.D.B. (DK41842 and DK51281).

* To whom correspondence should be addressed: Instituto de Física de São Carlos, Universidade de São Paulo, Av. Trabalhador Sãocarlense, 400, São Carlos, SP, Brazil 13560-970. Telephone: 55-16-273-8088. Fax: 55-16-273-9881. E-mail: ipolikarpov@if.sc.usp.br.

‡ Instituto de Física de São Carlos, Universidade de São Paulo.

§ Cornell University.

|| Instituto de Física, Universidade de São Paulo.

⊥ University of California.

[1] Abbreviations: TH, thyroid hormone; TR, thyroid hormone receptor; DBD, DNA binding domain; LBD, ligand binding domain; T_3, triiodothyronine; TREs, thyroid hormone response elements; NR, nuclear receptor; RXR, retinoid X receptor; IPs, inverted palindromes; SAXS, small-angle X-ray scattering; LB, Luria broth; IPTG, isopropyl thio-β-D-galactoside; PMSF, phenylmethanesulfonyl fluoride; SDS−PAGE, sodium dodecyl sulfate−polyacrylamide gel electrophoresis; Rf, retardation factor; R_H, hydrodynamic radii; DLS, dynamic light scattering; PDB, Protein Data Bank.

10.1021/bi061698h CCC: $37.00 © 2007 American Chemical Society
Published on Web 01/10/2007

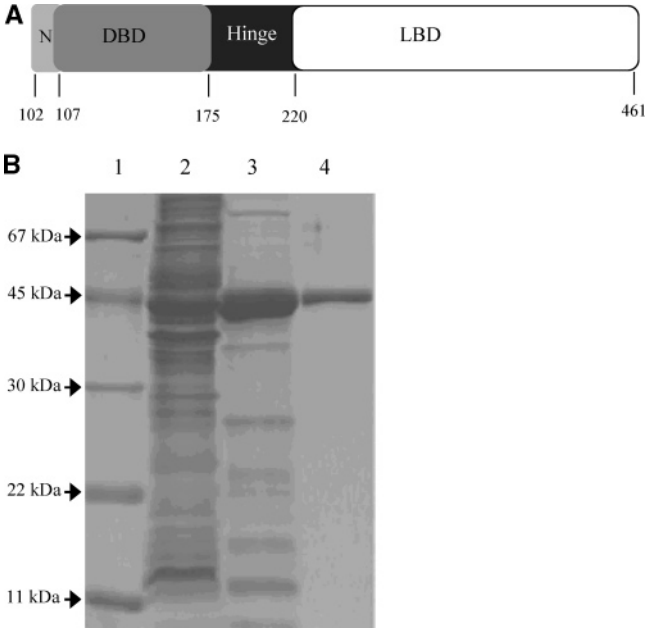

FIGURE 1: (A) TR DBD−LBD construct. The schematic illustrates the domains and amino acid composition: AAs, amino acids; N, N-terminal domain (A/B domain); DBD, DNA binding domain (C domain); hinge (D domain); and LBD, ligand binding domain (E domain). (B) TR DBD−LBD purification illustrated by 15% acrylamide gel electrophoresis of the TR DBD−LBD construct: lane 1, molecular weight markers; lane 2, soluble fraction after expression; lane 3, TR DBD−LBD elution pools after the affinity column, at the first step of purification; and lane 4, TR DBD−LBD elution pool after the gel filtration column, the last step of purification, where the protein is more than 95% pure. The arrows show the protein marker positions (67, 45, 30, 22, and 11 kDa). The position of the TR DBD−LBD band corresponds to 45 kDa, as expected.

X-ray structures of the TR DBD and holo LBD, along with structures of other NRs, have yielded important insights into TR and NR action (*13*−*15*). The TR DBD structure, obtained in complex with the RXR DBD on a TRE organized as a direct repeat of two half-sites spaced by four nucleotides (DR-4), confirms that TR occupies the 3′ half-site and highlights TR contact surfaces for DNA and the RXR (PDB entry 2NLL) (*16*). TR LBD structures reveal that the hormone is buried in the core of the domain, suggesting that large conformational changes accompany ligand binding. Use of these LBD structures to guide mutagenesis of the TR surface, along with analysis of X-ray structures of other NR LBD dimers and heterodimers in complex with different ligands and short coregulator peptides, has permitted definition of dimer−heterodimer and coregulator binding surfaces (*5*). Finally, X-ray structures of both domains revealed that many amino acids that were originally assigned to the D domain comprise α-helical extensions of the DBD and LBD (*17*, *18*).

In spite of these advances, much remains to be learned about the molecular basis of TR action. The TRs form several different oligomers with unique DNA binding preferences. In addition to RXR−TR heterodimers, which bind DR-4 elements, TRs bind to AGGTCA repeats arranged as inverted palindromes (IPs) as homodimers, to AGGTCA half-sites as monomers, and to tripartite TREs as trimers or heterotrimers (*7*, *19*). Our analysis of TRs in solution reveals more complexity (*20*). Previously, RXRs were thought to be unique among NRs in their capacity to form homotetramers; our studies indicate that TRs also form tetramers and, like RXR tetramers, that the TR tetramers are disrupted by incubation with cognate DNA elements or ligand (*21*−*23*). At present, TR LBDs have been crystallized in only monomeric form. While structure-directed mutagenesis confirms that formation of a RXR−TR heterodimer and a TR−TR homodimer involves the classic NR LBD dimer−heterodimer interface at the junction of helices (H) 10 and 11 (*3*, *11*), the organization of these TR oligomers and the reasons that they exhibit differences in their ability to bind to different TREs are completely unclear.

A better understanding of DBD−LBD relationships could also help clarify how DNA binding can influence transcriptional response. Thus, TR activates transcription from some TREs in the presence of T_3 yet represses transcription in response to T_3 binding at others (*1*). Further, the TRE sequence influences the magnitude of the T_3 response, the amount of T_3 required for half-maximal activation, the extent of basal repression by unliganded TRs at positive TREs, and the magnitude and direction of the response of TR to artificial ligands.

Finally, structures of unliganded TRs are not available, and only a few structures of unliganded NR LBDs have ever been determined (*24*−*29*). Targeted mutagenesis experiments have shown that T_3 promotes coregulator exchange by repositioning the LBD C-terminal H12 (*8*, *10*) and disrupts TR−TR homodimer formation on DNA by remodeling homodimer specific extensions of the classic LBD dimer interface (*12*). Nevertheless, the effects of hormone upon LBD structure and the spatial relationships between individual domains are completely unclear (*5*, *14*, *15*).

While no high-resolution structures of TRs or other NR DBD−LBD constructs are yet available in any form, we have been able to determine the structure of the RXR DBD−LBD region at low resolution using synchrotron X-ray solution scattering (SAXS) (*30*). The technique reveals the structure of macromolecules in solution at nanometer resolution and can be used to determine likely positions and orientations of individual domains. Here, we present the first low-resolution structures of the TRβ DBD−LBD construct in the dimer and tetramer forms. The data reveal that liganded TR predominantly forms dimers and unliganded TRs predominantly form tetramers. While there are striking similarities between TR and RXR DBD−LBD constructs, there are also differences. RXR DBD−LBD tetramers are X-shaped, with four DBDs widely spaced and extended from the LBD core (*30*), whereas TR DBDs are closely packed together along the symmetry axis of the TR LBD tetramer, yielding an elongated cigar-shaped assembly. We suggest that this organization points to unsuspected DBD−DBD and LBD−DBD interactions in the TRs. Our results also indicate that hormone-dependent conversion of TR homotetramers to TR dimers is an allosteric event triggered by T_3 binding.

EXPERIMENTAL PROCEDURES

Protein Expression and Purification. Human TRβ DBD−LBD cDNA [residues 102−461 (Figure 1A)] fused in frame to the C-terminus of a polyhistidine (His) tag in a pET28a-(+) plasmid (Novagen) was expressed in *Escherichia coli* strain BL21(DE3). A Luria broth (LB) starter culture was

inoculated with a single colony of a LB agar culture and grown overnight at 37 °C. The initial culture was inoculated at 1% in a major 2XYT culture and grown at 22 °C in kanamycin medium until the A_{600} reached 1.5. Protein production was initiated with 1 mM isopropyl thio-β-D-galactoside (IPTG), and the culture was incubated for 4 h at 22 °C. The induced cultures were harvested by centrifugation, and the pellets were resuspended in 50 mM Tris-HCl (pH 8.0), 150 mM NaCl, 0.05% Tween 20, and 20 mM β-mercaptoethanol. Phenylmethanesulfonyl fluoride (PMSF) and lysozyme were added to final concentrations of 1 mM and 250 μg/mL, respectively, and the culture was placed on ice for 30 min. The lysate was sonicated and clarified by centrifugation for 1 h at 14 000 rpm in a Sorvall SS34 rotor at 4 °C. The supernatant was incubated in batch with 1 mL of Talon Superflow Metal Affinity Resin (Clontech) per liter of culture for 1 h at 4 °C. The resin was washed with 50 mM sodium phosphate buffer (pH 8.0), 300 mM NaCl, 10% glycerol, 0.05% Tween 20, and 10 mM β-mercaptoethanol. The bound TRβ1 protein was eluted with 50 mM sodium phosphate buffer (pH 8.0), 300 mM NaCl, 10% glycerol, 0.05% Tween 20, 10 mM β-mercaptoethanol, and 500 mM imidazole in a single step. After this step, the protein was loaded into the gel filtration HL Superdex 200 16/60 column (GE Healthcare) equilibrated with 20 mM Hepes-Na buffer (pH 8.0), 3 mM dithiothreitol, 400 mM NaCl, and 5% glycerol.

After purification, the His tag was removed by incubation with thrombin at the concentration 10 units/mg of protein, for 5 h at 18 °C. To produce holo TR, T_3 (3,5,3′-triiodo-L-thyronine, Sigma) was added after cleavage to a 10-fold molar excess and the mixture incubated for 0.5 h at 4 °C. The liganded protein was concentrated by ultrafiltration (Amicon Ultra 10MWCO, Millipore).

The average yield of the protein, with a purity of >95%, is 3−5 mg/L of culture. The protein content and purity of all chromatographic fractions were verified at each stage by Coomassie Blue-stained sodium dodecyl sulfate−polyacrylamide gel electrophoresis (SDS−PAGE). The protein concentration was determined using the Bradford dye assay (Bio-Rad) and bovine serum albumin as a standard.

Native Polyacrylamide Gel Electrophoresis. An apo hTRβ DLD−LBD construct, at a concentration of 2 mg/mL (50 μM), was electrophoresed on an 8 to 25% (w/v) pH 8.8 gradient polyacrylamide gel using the Phast System (GE Healthcare), at 4 °C, and Coomassie-stained following standard protocols (*20*). The protein was incubated with cognate ligand, T_3 (at 0, 0.125, 0.25, 0.5, 0.75, 1.0, and 3.0 times the molar concentration of the receptor), and electrophoresed to assess the oligomeric state. Protein standards of known hydrodynamic radii (thyroglobulin, 8.5 nm; ferritin, 6.1 nm; catalase, 5.22 nm; lactate dehydrogenase, 4.3 nm; and bovine serum albumin, 3.55 nm) were electrophoresed under the same conditions. The mobilities of the individual bands of the protein standards were plotted as the retardation factor (Rf) versus the hydrodynamic radii (R_H) (*20*). The linear equation obtained from this calibration was employed to calculate the R_H of the multimeric fractions of the hTRβ1 DBD−LBD construct.

Dynamic Light Scattering. Dynamic light scattering (DLS) was used to determine the hydrodynamic radius of the TR at different concentrations, in its apo and holo form, and to evaluate sample monodispersity. The R_H is given by the Stokes−Einstein relation:

$$R_H = (k_B T)/(6\pi\eta D)$$

where k_B, T, η, and D are the Boltzmann constant, absolute temperature, solvent viscosity, and diffusion coefficient, respectively. As the hydrodynamic radius is much smaller than the wavelength ($R_H \ll \lambda$), a spherical particle at extrapolated zero concentration will have its volume V related to R_H so that $V = {}^4/_3\pi R_H{}^3$. An average molar mass can be then calculated by

$$M = (V/\upsilon)N_A$$

where υ is the protein partial specific volume and N_A is Avogadro's number.

DLS measurements were carried out in an experimental buffer of 20 mM HEPES buffer (pH 8.0), 300 mM NaCl, 3 mM DTT, and 5% glycerol using a DynaPro MSTC014 instrument (Protein Solutions Inc., Lakewood, NJ). The assays were performed at 4 °C with an acquisition time of 2.5 s using a 12 μL cuvette. Thirty acquisitions were averaged in a single measurement. Five sequential measurements were performed for each concentration of the apo and holo form of the TRβ DBD−LBD construct, and the mean and the standard deviations were computed. Changes in viscosity, introduced by glycerol present in solution (5%), were taken into account during evaluation of the hydrodynamic radii of TR multimers by DYNAMICS version 5.26.39 (Protein Solutions Inc.).

Hydrodynamic radii were transformed to R_G by the simplified relationship $R_H = R_G \times 1.3$ (*31*). Experimental data were compared to hydrodynamic properties calculated from the low-resolution structure using HYDRO (*32*).

Small-Angle X-ray Scattering Measurements and Data Analysis. SAXS data were collected at the small-angle scattering beamline on the LNLS (National Synchrotron Light Laboratory, Campinas, Brazil) using a one-dimensional position-sensitive detector (*33*), and the TRβ1 DBD−LBD construct at 3, 5, and 8 mg/mL was measured at a wavelength (λ) of 0.148 nm for sample−detector distances of 1030.3 mm covering the momentum transfer range (q) of 0.1−3 nm^{-1} ($q = 4\pi \sin\theta/\lambda$, where 2θ is the scattering angle). The scattering curves of the protein solutions and the corresponding solvents were collected in a number of short frames to monitor radiation damage and beam stability. The data were normalized to the intensity of the incident beam and corrected for detector response.

The scattering of the buffer was subtracted, and the curves were scaled for concentration. The distance distribution functions [$p(r)$] and the radii of gyration (R_g) were evaluated by the indirect Fourier transform using GNOM (*34*).

Prior to the shape analysis, a constant was subtracted from the experimental data to ensure that the intensity at higher angles decays as q^{-4} following Porod's law for homogeneous particles (*35*). The value of the constant is derived automatically from the outer part of the curve by linear fitting in coordinates $q^4I(0)$ versus q^4 by the shape determination program DAMMIN (*36*). This procedure reduces the contribution from scattering due to the internal protein structure and yields an approximation of the "shape scattering" curve

(i.e., scattering from the excluded volume of the particle filled with a constant density).

The experimental pair distribution functions do not contain any negative part, indicating that the interference effects in the scattering curves produced by spatial correlations were absent and that all solutions were sufficiently dilute. The structure function that describes interparticle correlations may be equal to unity even at high concentrations for proteins of very anisotropic shape (*37*).

Ab Initio Shape Determination of hTRβ1 DBD−LBD Dimers and Tetramers. Low-resolution particle shapes were restored from the experimental SAXS data using two independent ab initio procedures. In the first approach (*38*, *39*), the shape is described by an angular envelope function, parametrized in terms of spherical harmonics using multipole expansion techniques (*40*). The maximum number of spherical harmonics is chosen so that the number of free parameters is close to the number of Shannon channels in the experimental data (*41*). The envelopes were represented with spherical harmonics up to $L = 4$ (13 independent parameters) for both dimers and tetramers of the hTRβ1 DBD−LBD construct. This was justified by the fact that the portions of the scattering curves used for ab initio shape determination using the envelope functions contained $N_S = 5$ and $N_s = 10$ Shannon channels for the hTRβ1 DBD−LBD dimer and tetramer, respectively. The 2-fold symmetry was assumed for the hTRβ1 DBD−LBD dimer and 222 symmetry for the hTRβ1 DBD−LBD tetramer, resulting in a significant reduction in the number of free parameters of the models.

Particle shapes were also calculated from the SAXS data using the ab initio procedure implemented in DAMMIN (*36*). In a first step, the calculation was conducted without symmetry restraints (data not shown) and, in a second step, using the same symmetry restraints as in the previous approach. Low-resolution ab initio TR molecular envelopes retrieved from SAXS data without any symmetry constraints rendered essentially the same molecular shapes as the envelopes computed with use of these constraints. Application of the symmetry constraints, however, did result in a significant reduction in a number of free parameters of the models. Several lines of experimental evidence also support application of 2-fold symmetry of TR dimers and 222 point symmetry of TR tetramers. Most nuclear receptors form functional dimers [homodimers or heterodimers with the retinoid X receptor (RXR)] (*5*) or tetramers (*42*−*45*). Available homodimer and heterodimer structures display 2-fold symmetry and use the same dimerization interface (*11*, *24*, *25*, *46*). Moreover, known RXR and ER homotetramers form dimers of dimers and display 222 point symmetry (*47*−*49*). Finally, previous RXR LBD and RXR DBD−LBD solution small-angle scattering data are consistent with 2-fold symmetry for dimers and 222 point symmetry for tetramers (*30*, *50*).

With this approach, a sphere with a diameter of D_{max} is filled with densely packed small spheres (dummy atoms) where radius $r_0 \ll D_{max}$. The search volume for the hTRβ1 DBD−LBD dimer was filled with 6603 dummy atoms (N_{DAM}) with a packing radius (r_a) of 0.29 nm within a sphere with a diameter D_{max} of 12.0 nm. The search volumes for the hTRβ1 DBD−LBD tetramer were filled with 7376 dummy atoms (N_{DAM}) with a packing radius (r_a) of 0.42 nm within a sphere with a diameter D_{max} of 18.0 nm. Twenty independent ab initio simulations were performed. Of those, 182 ± 10 dummy atoms were assigned to the final model of the hTRβ1 DBD−LBD dimer and 590 ± 30 dummy atoms to the hTRβ1 DBD−LBD tetramer. Average models were calculated with the DAMAVER package programs (*51*). DAM-derived radii of gyration are in agreement with the experimental R_g obtained from DLS data (see Results).

Structural Model Building. Sets of coordinates for the hTRβ1 DBD and LBD were obtained from the Protein Data Bank (PDB entries 2NLL and 1NAX) (*16*, *52*), and a full DBD−LBD construct was modeled using Modeller (*53*). The tetramer and dimer were generated by superimposition of four hTRβ1 LBDs onto the hRXRα LBD tetramer (PDB entry 1G5Y) (*47*) and two hTRβ1 LBDs onto the hRXRα LBD dimer (PDB entry 1G5Y), respectively, using Superpose (CCP4 package) (*54*). The oligomers were manually adjusted using Coot (*55*) to avoid clashes. Relative positions of the DBD domains were found by iterative rotation of their envelope functions to minimize the discrepancy with the ab initio low-resolution structure. The models were displayed using MASSHA (*56*). Radii of gyration (R_g), maximum intraparticle distances (D_{max}), envelope functions, and scattering curves were calculated from these atomic coordinates by using CRYSOL taking into account the influence of the hydration shell (*57*).

RESULTS

Hormone-Dependent Conversion of the TRβ DBD−LBD Tetramer to Dimers. We first obtained purified preparations of the TRβ DBD−LBD construct in the presence and absence of hormone and characterized the oligomeric state of TR under both conditions. While SDS−PAGE confirms that the TRβ DBD−LBD preparations comprise a single species of the expected molecular weight (Figure 1B), nondenaturing gel analysis (Figure 2) and dynamic light scattering (DLS) reveal that the unliganded TRβ DBD−LBD construct exists in a form that is significantly larger than the liganded TRβ DBD−LBD construct and that the approximate sizes of these species correspond to tetramers and dimers, respectively. The data confirm our previous findings, based on native gel electrophoresis, chemical cross-linking, analytical gel filtration, and DLS experiments, that liganded TRβ forms dimers and unliganded TRβ forms tetramers (*20*).

Hormone-dependent dissociation of TR tetramers from dimers is shown in Figure 2A. Titration of the hTRβ1 DBD−LBD construct with the increasing concentrations of T_3 results in the disappearance of the tetramer band (lanes 1 and 2) and the appearance of the dimer band (lanes 3−7). Remarkably, dissociation of tetramers required only T_3 at a molar ratio of one-fourth of that of the receptor. Thus, binding of only one hormone molecule to the hTRβ1 DBD−LBD tetramer is required for dissociation of this multimeric assembly, suggesting that a single holo receptor must exert allosteric effects on its partners that are sufficient to disrupt the TR tetramer interface.

Dynamic light scattering (DLS) analysis underscores the notion that TRs remain monodisperse at several different concentrations (1, 3, 5, and 8 mg/mL) yet form species of different sizes in the absence and presence of T_3 (not shown). Thus, unliganded TR exhibits an experimental radius of gyration (R_g) of 4.6 ± 0.3 nm, whereas the T_3-liganded

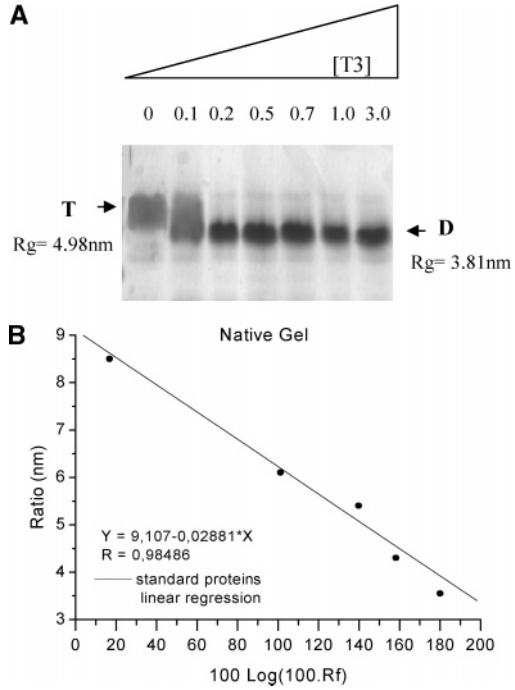

FIGURE 2: Native polyacrylamide gel electrophoresis shows tetramer dissociation. The native gel of the hTRβ DBD−LBD construct shows the tetramer dissociation after addition of T_3. (A) Dissociation of apo TR tetramers after addition of 0, 0.125, 0.25, 0.5, 0.75, 1.0, and 3.0 M T3. Binding of only one hormone molecule to the hTRβ1 DBD−LBD tetramer is required for dissociation of this multimeric assembly (lane 3) which indicates the presence of allosteric effects. This gel was stained with Coomassie corant blue. (B) Calibration curve of standard proteins that were electrophoresed under the same conditions to evaluate the radii of TR species (Experimental Procedures).

form exhibits an R_g of 3.5 ± 0.2 nm. Both of these values are consistent with the notion that the unliganded TRβ DBD−LBD construct forms tetramers and that the liganded TRβ DBD−LBD construct forms dimers. We previously determined that TR tetramers also dissociate upon incubation with cognate TREs (*20*). Thus, our data strengthen the hypothesis that unliganded TRs form tetramers and suggest that tetramerization is associated with formation of an inactive state of the receptor that can be activated by ligand or DNA binding.

Ab Initio Models of TRβ DBD−LBD Tetramers and Dimers. To analyze the overall shape of T_3-liganded TRβ dimers and unliganded tetramers, we performed SAXS analysis of the TRβ DBD−LBD construct at a range of different protein concentrations in the presence and absence of T_3. Typical scattering curves obtained with the TRβ DBD−LBD preparations are presented in panels A and B of Figure 3, and structural parameters derived from these curves are given in Table 1. The data indicate that the maximum intraparticle distance (D_{max}) and radius of gyration (R_g) of unliganded TRs are 18.0 and 4.9 nm, respectively, whereas liganded TR forms a species with a D_{max} of 12 nm and an R_g of 3.8 nm. These results are in good agreement with the parameters derived from DLS studies ($R_g^{tetramer}$ = 4.6 nm and R_g^{dimer} = 3.5 nm) and also suggest that both species are relatively elongated. Indeed, the maximum intraparticle distances are 3−4 times greater than radii of gyration for both TR DBD−LBD dimers and tetramers. This notion is further supported by profiles of the distance

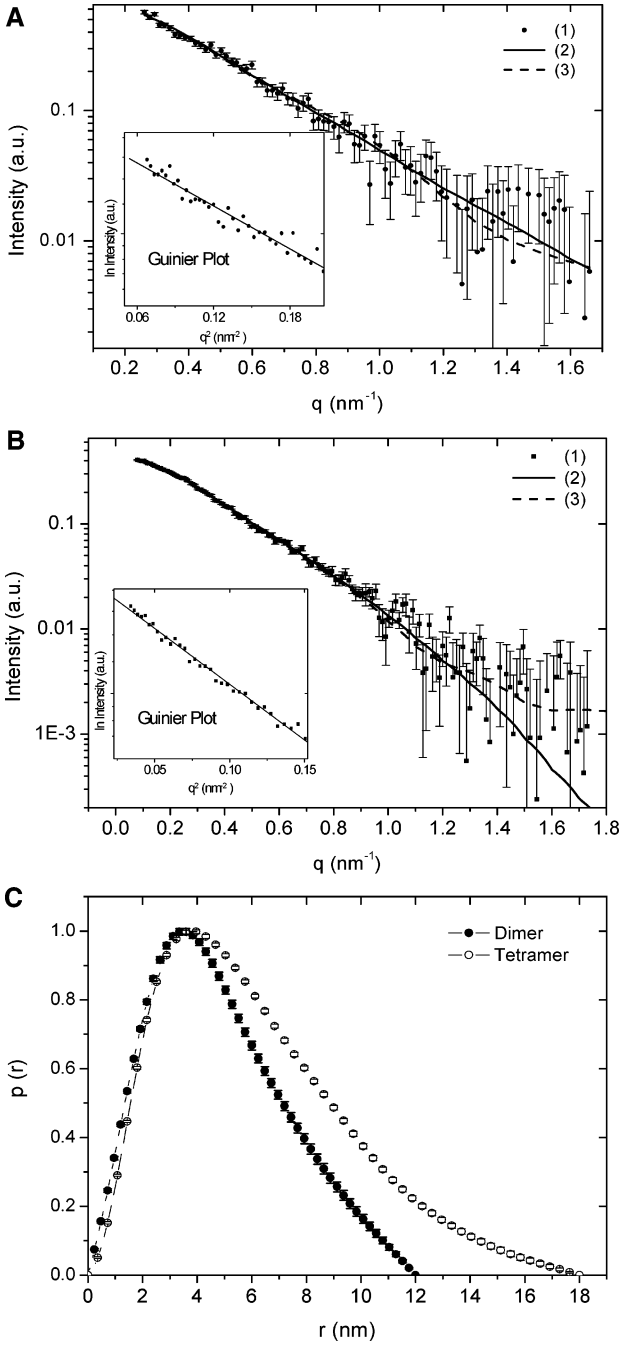

FIGURE 3: Experimental solution scattering curves of the hTRβ1 DBD−LBD construct, results of the fitting procedures, and distance distribution functions: (A) dimer and (B) tetramer. Log I vs q focusing on the fitting of the experimental curve at high q values with an inset containing the corresponding Guinier plots (log I vs q^2): (1) experimental curve, (2) scattering intensity from the DAMs [DAMMIN (36)], and (3) scattering intensity from the high-resolution models. (C) Distance distribution functions of hTRβ1 DBD−LBD dimers (○) and tetramers (●) are given.

distribution function [$p(r)$] in Figure 3C, which are typical of elongated particles (*35*, *37*).

Overall shapes of unliganded and liganded TRβ DBD−LBD species were determined ab initio by two independent procedures (Materials and Methods) and are presented in Figure 4. Both independent ab initio reconstructions rendered very similar molecular forms. The holo TRβ DBD−LBD constructs have a palm-shaped tertiary structure (Figure 4A), whereas apo TRβ DBD−LBD constructs form molecular assemblies which resemble slightly distorted cigars (Figure

Table 1: Structural Parameters Derived from SAXS Data

	hTRβ1 DBD−LBD dimer			hTRβ1 DBD−LBD tetramer		
	exp.[a]	mod.[b]	DAM[c]	exp.[a]	mod.[b]	DAM[c]
D_{max}	12.00 ± 1.00	12.80	12.10	18.00 ± 1.00	18.61	17.84
R_g (nm)	3.79 ± 0.50	3.82	3.66	4.97 ± 0.50	4.96	4.84
free parameters	5[d]	−	3301[e]	10[d]	−	1844[f]
discrepancy χ	−	0.9	0.9	−	1.2	1.1
resolution (nm)	3.8	−	3.8	3.5	−	3.5

[a] Calculated from the experimental data. [b] Parameters of the dimer and tetramer models. [c] Parameters of the dummy atom models averaged over 20 models. [d] The number of Shannon channels is given. $N_s = (q_{max}D_{max})/\pi$. [e] Two-fold symmetry imposed. [f] Symmetry *P*222 imposed.

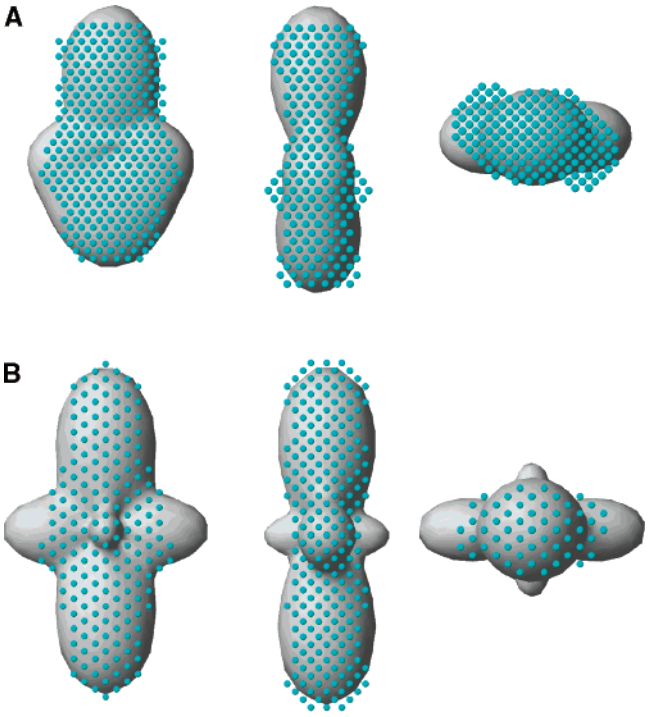

FIGURE 4: SAXS envelopes for the liganded and unliganded TRβ DBD−LBD construct derived from ab initio calculations. SAXS ab initio envelopes for holo TRβ DBD−LBD dimers (A) and apo TRβ DBD−LBD tetramers (B). Molecular envelopes obtained by spherical harmonics expansion [SASHA (*38*, *39*)] are shown as a gray solid surface, and the dummy atom models obtained by DAMMIN (*36*) are depicted as blue spheres. Three orthogonal views of the same envelopes are given.

4B). Apo TRβ DBD−LBD tetramers are significantly more elongated, consistent with their greater molecular weight, but are somewhat too short to accommodate two holo TRβ DBD−LBD dimers in a head-to-head arrangement (not shown). This suggests that there must be significant alteration in the respective positions of the DBD and LBD in the dimer and tetramer forms.

Structural Model of the TRβ DBD−LBD Dimer. To determine likely relative positions and orientations of the TRβ DBDs and LBDs in our low-resolution dimer structures, we created structural models of holo TRβ DBD−LBD dimers based on previously published high-resolution X-ray structures of these domains and analyzed the fit of the models within the TRβ DBD−LBD molecular envelope. In line with the ab initio SAXS-derived low-resolution structures, we assumed 2-fold symmetry of the TR DBD−LBD dimer models along the long axis, passing through the center of the envelope. Sequences corresponding to the D domain, which links the DBD and LBD, were modeled as an extended α-helix (see Discussion).

The best fit for the TRβ DBD−LBD dimer model, superimposed upon the SAXS palm-shaped envelope for the dimer, is shown in Figure 5. The LBDs lie at the base of the palm and occupy a volume consistent with predicted tail-to-tail symmetric homodimer interactions mediated by the LBD H10−H11 dimer interfaces. Analysis of the best fit for the TR DBDs indicates that they are at the top of the molecule ("finger region" of the palm), extended from the LBDs. Here, the D domain that links the two domains must be relatively extended; the overall separation of the LBD and the DBD is consistent with the notion that the D domain forms a relatively continuous extended α-helix that is analogous to our artificial linked DBD−LBD structural models and partly suggested by our previous crystallographic models of the TR D domain−LBD region (*18*). The DBDs are in close contact, raising the possibility that they may engage in hitherto unexpected intermolecular contacts.

Placement of the DBD structural models within the molecular envelope suggests that the best fit is to a tail-to-tail orientation suitable for binding to inverted palindromic (IP) TREs, the preferred binding site for TR homodimers (*5*). The resolution of the molecular envelope [~3.5 nm resolution (Table 1)] is not sufficient to directly distinguish the relative orientations of the DBDs. Nevertheless, we find that the D domains overlap in the tail-to-tail (inverted palindrome) orientation and that these intermolecular contacts do not occur in the head-to-head (palindrome) orientation, resulting in a weaker putative homodimer (not shown). While it is conceivable that DBDs could be oriented asymmetrically, as would be required for binding to asymmetric DR-4 elements, we also find that D domain contacts would not be available in these orientations (not shown). Thus, the best prediction from our low-resolution model suggests that the DBD−LBD homodimer adopts a conformation with DBDs positioned for binding to inverted palindromes and that intermolecular contacts between the DBDs and D domains contribute to homodimer formation (see Discussion).

Structural Model of the TRβ DBD−LBD Tetramer. Next, we analyzed likely positions of TR domains in the apo TR tetramer molecular envelope. The best fit was obtained by positioning four LBDs in the center of the molecule in a form that resembles previously published structures of RXR LBD tetramers. Here, two LBD pairs are stacked on top of each other, and the LBD dimer pairs are oriented at an angle of 180° with respect to each other. The DBD pairs protrude from the core in two opposite directions such that the overall predicted tetramer resembles a bulged cylinder (Figure 6). Like the organization of DBDs in the TR homodimer, the two DBDs that form each pair at the extremities of the cylinder are in close contact with each other. This organiza-

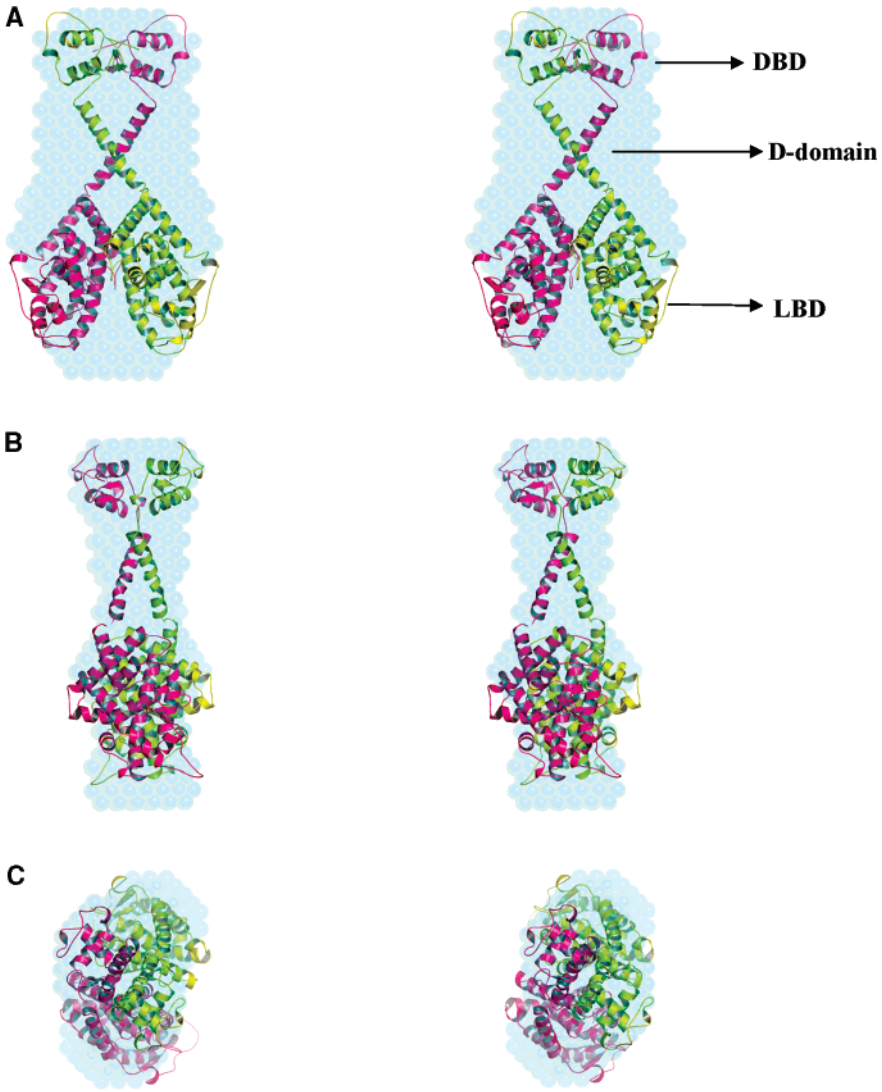

FIGURE 5: hTR βDBD−LBD dimer high-resolution models. Panels A−C show three orthogonal stereoviews of the superposition of an average of 10 independent DAMs of the holo hTRβ DBD−LBD dimer, obtained by an ab initio procedure as implemented in DAMMIN (*36*) and its three-dimensional model composed of X-ray structures of two hTRβ DBDs (*16*) and two hTRβ1 LBDs (*52*).

tion differs from our low-resolution structures of RXR tetramers, which were X-shaped with DBDs widely spaced (*30*), and represents further evidence that the TR DBDs may engage in unique intermolecular contacts.

DISCUSSION

In this study, we report low-resolution [~3.5 nm resolution (Table 1)] structures of the TRβ DBD−LBD construct in solution in the absence and presence of cognate ligand T_3. The structures confirm our previous suggestion that the liganded TR DBD−LBD constructs form dimers and that unliganded TRs form tetramers (*20*) and provide insights into the organization of both forms. The data raise the possibility that there are hitherto unappreciated interactions between TR domains and that the ligand-dependent oligomeric state of the TR exerts strong influences upon the relative position of the TR DBD and LBD.

The low-resolution structure of liganded TR confirms that it is a dimer with an overall shape that conforms to previous predictions about the organization of these species. TR dimers are palm-shaped. Fitting of high-resolution models (~0.2 nm resolution) of the LBD and DBD into the molecular envelope suggests that the LBDs are in close contact at the base of the palm and DBDs at the fingers region, extended from the LBD. Juxtaposition of LBDs is consistent with the predicted role of LBD−LBD contacts in TR homodimer formation (*5*, *11*). Moreover, the shape and separation of the DBD and LBD are similar to those observed in low-resolution structures of the RXR DBD−LBD construct (*30*) (Figure 7).

Several features of TR dimers are distinct from those of RXR dimers (Figure 7). Most notably, the TR DBDs are closely juxtaposed, and the D domain−hinge regions interact. In our previous low-resolution RXR dimer structures (*30*), RXR DBDs were spaced ~2 nm apart at an angular separation of 10°. This close juxtaposition of DBDs and hinge domains in the TRs raises the possibility that these regions engage in homodimer specific contacts that supplement LBD−LBD interactions and/or help to position the DBDs in an appropriate configuration for DNA binding. Accordingly, our preliminary data indicate that a bacterially expressed TRβ protein fragment that contains the DBD and part of the D domain−hinge motif also dimerizes in solution at typical protein concentrations required for SAXS analysis

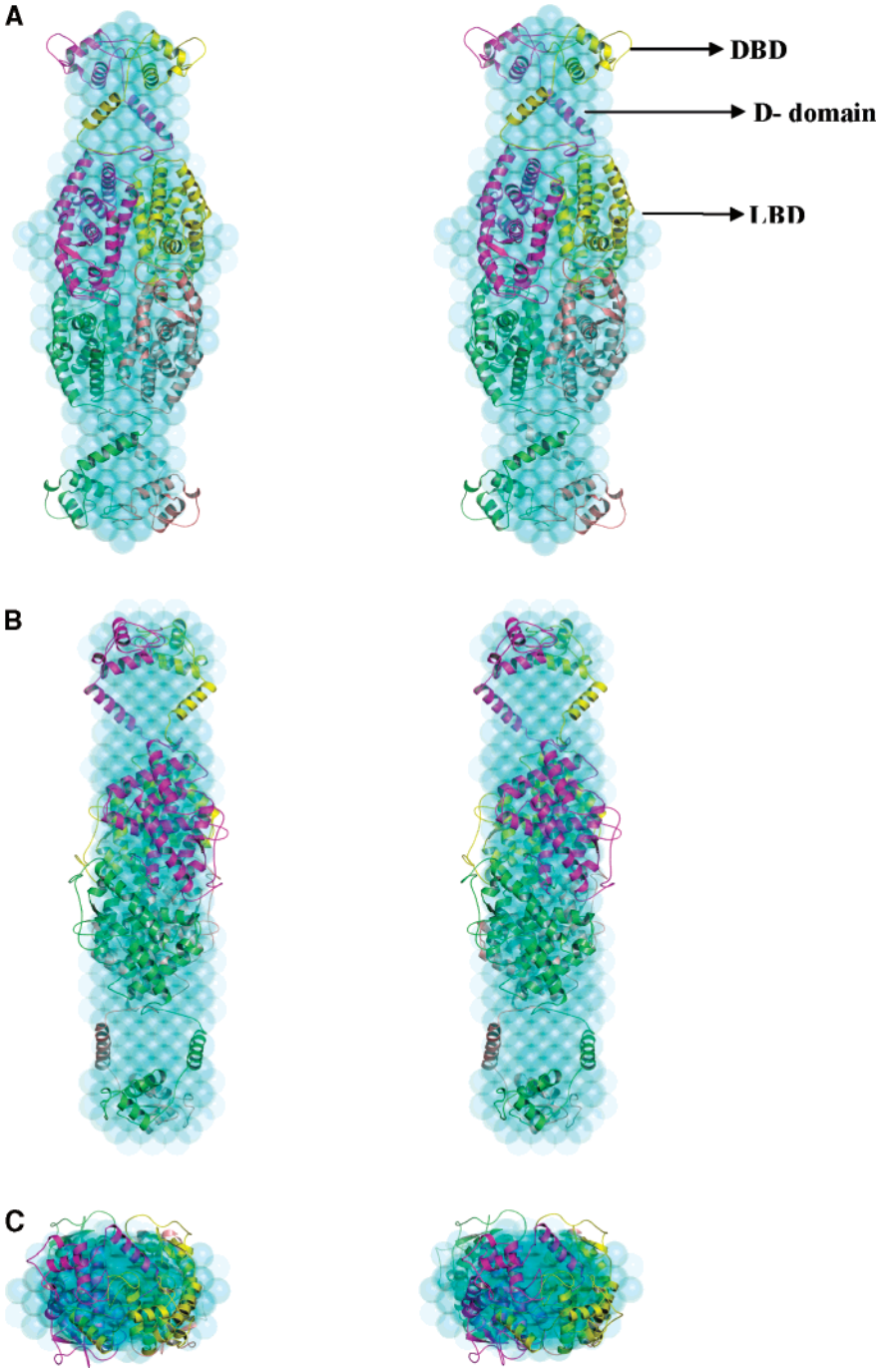

FIGURE 6: hTRβ DBD−LBD tetramer high-resolution models. Panels A−C display three orthogonal stereoviews showing the best superposition of the average of 10 apo hTRβ DBD−LBD tetramer DAMs obtained by ab initio simulations using protocols implemented in DAMMIN (*36*) and its three-dimensional model of X-ray structures of four hTR β DBDs (*16*) and four hTR β1 LBDs (*52*).

(not shown). Some previous studies suggested that TR DBDs may engage in homodimer specifc contacts at palindromes (reviewed in ref *7*), but later studies revealed that true homodimers do not form at these elements (*11*). It is interesting to suggest that the D domain contacts predicted by our low-resolution structures could play a role in this phenomenon.

The predicted structure of the unliganded TR corroborates our previous finding that it is the size and shape of a tetramer (*20*) and further suggests that it may resemble RXR tetramers (*30*). The unliganded TRs adopt an elongated conformation that resembles a slightly bulged cylinder, or cigar, with four LBDs at the core of the molecule and two pairs of DBDs protruding in either direction in an extended conformation. RXR tetramers are formed by head-to-head interactions between pairs of LBD dimers rotated at 180° with respect to each other (*47*). Our TR structures confirm that the tetramer interface also involves LBD−LBD contacts, and a TR LBD tetramer model based on RXR LBD tetramer coordinates (*47*) fits well into the low-resolution envelope. The RXR tetramer interface involves H3 and H11 at the base of the LBD, with additional contacts between C-terminal H12 and the H3−H5 region of the neighboring subunit (*47*). Here, ligand-dependent repositioning of H12 completes the coactivator binding surface and disrupts tetramers (*25*, *42*, *43*). It is intriguing to speculate that TRs adopt a similar

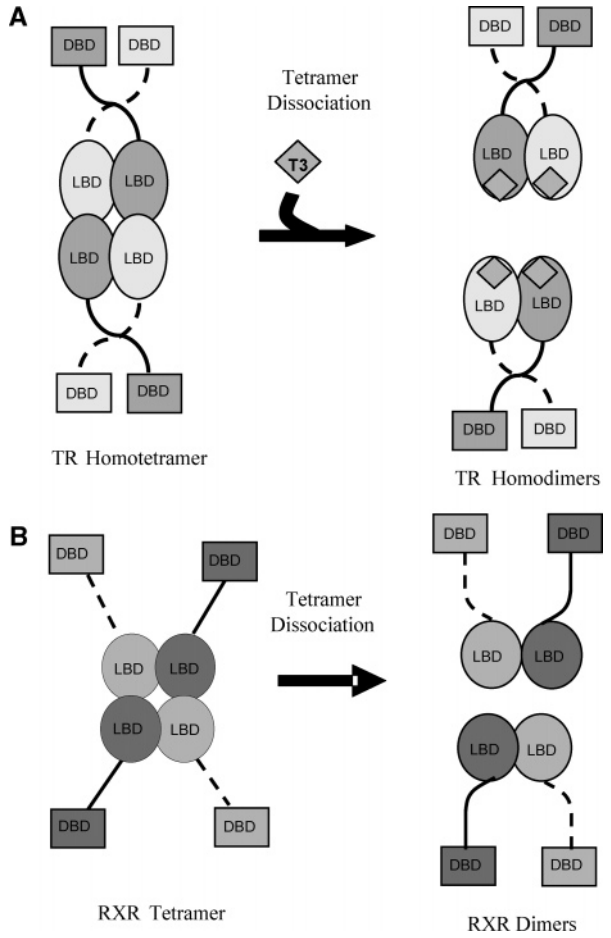

FIGURE 7: Diagram of TR and RXR dimers and tetramers. (A) The apo hTRβ DBD−LBD construct forms tetramers that resemble bulged cylinders with pairs of LBD dimers in head-to-head arrangement with DBD pairs packed tightly against the LBD core. The TR tetramers dissociate into dimers upon ligand binding or DNA binding, and/or heterodimerization with the RXR. The holo hTRβ DBD−LBD construct forms a homodimer with LBD−DBD pairs in close contact and DBDs protruding from the base in the same direction. The DBDs are connected to the LBDs by crossed extended D domains. (B) hRXRα DBD−LBD dimer and tetramer models proposed by Fischer et al. (*30*). The apo RXR tetramers are more elongated X-shaped molecules formed by two dimers in a head-to-head arrangement with the DBDs extended from the structure. The apo RXR dimers are U-shaped with DBDs in a head-to-head orientation and with an extensive interface area provided by the LBDs, and their D domains are not crossed (*30*).

organization and undergo similar rearrangements that would account for ligand-dependent dissociation of TR tetramers.

There are marked differences in the spacing of DBDs and LBDs in the TR dimer and tetramers, just as we previously observed differences in DBD−LBD spacing in RXR dimers and tetramers (*30*) (Figure 7). TR LBDs and DBDs are widely separated in the dimer, but both TR DBD pairs are close to the LBD core in tetramers. The tetramer organization could preclude DNA binding because the DBDs are packed against the LBD and not available for DNA contact. In addition, the best fit of DBDs in the tetramer envelope suggests that they are in a head-to-head orientation and therefore not in a configuration that would bind IP and DR-4 elements that are typical of native TREs. Thus, dimer−tetramer interactions at the LBD seem to alter the distance between the DBD and LBD and, possibly, their relative orientations. This finding may explain our previous observation that TR tetramers tend to dissociate to form dimers after incubation with cognate-inverted palindromic TREs (*20*). In spite of these similarities, the precise details of the organization of TR tetramers do differ from those of RXRs. Whereas TR DBDs are closely juxtaposed and packed against the LBD, RXR DBDs were extended from the LBD core in the tetramer and widely spaced with respect to each other (6 nm) (*30*). While both conformations would tend to preclude DNA binding, this finding lends further support to the notion that there are differences in TR and RXR organization.

Our structures do not explain how dimer and tetramer interactions at the LBD can alter DBD position, but we suggest that there are two possible influences. First, TR could engage in interdomain interactions not available to RXRs, and TR DBDs could interact both with each other and with the LBD in the tetramer. Second, analysis of the apparent separation of DBDs and LBDs suggests that the D domain likely forms an extended α-helix in the dimer, consistent with our previous high-resolution X-ray structures of D domain LBD regions (*18*), but that the two domains are tightly packed in the tetramer. Thus, protein−protein interactions at the LBD also seem to influence the position and/or conformation of the D domain (*18*). Such reorganization corroborates our previous findings of D domain rearrangements in high-resolution X-ray crystallographic structures of TRα and TRβ fragments and suggests that this influence could provide rotational flexibility required for recognition of different DNA elements and for formation of different TR oligomers (*18*).

Finally, while evidence of the physiological relevance of TR homodimers and tetramers is limited, our structures permit some predictions about the possible function of these TR oligomers. Whereas TRs generally heterodimerize with RXRs in living cells, there are indications that unliganded TR homodimers mediate transcriptional repression at positive TREs and T_3-dependent transcriptional activation at IPs and variant DR-4 elements (*5*, *58*, *59*). That the TR DBD−D domain regions may engage in homodimer specific contacts lends support to a putative physiological role for this species. The apparent structural similarity between RXR and TR tetramers suggests that these species fulfill similar functions (*20*−*23*, *30*, *42*−*45*, *50*, *58*−*61*). It is proposed that RXR tetramer formation acts as an autosilencing mechanism, and accordingly, RXRα mutations that inhibit tetramer formation lead to constitutive activity (*43*, *62*, *63*). Since unliganded TRs form complexes with corepressors (*8*), the requirement for a second autosilencing mechanism is not obvious. RXR tetramer formation is also proposed to permit interactions with unusual response elements with widely spaced half-sites (*44*, *45*), and since native TREs are often complex (*64*−*66*), it is interesting to speculate that TR tetramers could modulate transcription from unusual variant TREs. Indeed, cooperative binding and correlated synergistic activation of transcription from response elements with four half-sites have also been reported for estrogen (*67*), progesterone (*68*), and glucocorticoid (*69*) receptors. Further investigation will be required to define the function of TR tetramers, if any. Nevertheless, the fact that TRs form tetramers indicates that RXRs are not unique in this capacity and raises the possibility that other NRs could form tetramers under appropriate conditions or promoter contexts.

ACKNOWLEDGMENT

We thank Laboratório Nacional de Luz Síncrotron (LNLS) for access to SAXS beamline and other facilities.

REFERENCES

1. Yen, P. M. (2001) Physiological and molecular basis of thyroid hormone action, *Physiol. Rev. 81*, 1097−1142.
2. Lazar, M. A. (1993) Thyroid hormone receptors: Multiple forms, multiple possibilities, *Endocr. Rev. 14*, 184−193.
3. Aranda, A., and Pascual, A. (2001) Nuclear hormone receptors and gene expression, *Physiol. Rev. 81*, 1269−1304.
4. Cheng, S.-Y. (1995) New insights into the structure and function of the thyroid hormone receptor, *J. Biomed. Sci. 2*, 77−89.
5. Laudet, V., and Gronemeyer, H. (1995) *The Nuclear Receptors Facts Book*, pp 1−109, Academic Press, London, U.K.
6. Baxter, J. D., Webb, P., Grover, G., and Scanlan, T. S. (2004) Selective activation of thyroid hormone signaling pathways by GC-1: A new approach to controlling cholesterol and body weight, *Trends Endocrin. Metab. 15*, 154−157.
7. Desvergne, B. (1994) How do thyroid hormone receptors bind to structurally diverse response elements, *Mol. Cell. Endocrinol. 100*, 125−131.
8. Glass, C. K., and Rosenfeld, M. G. (2000) The coregulator excahange in transcription function of nuclear receptors, *Genes Dev. 14*, 121−141.
9. Feng, W. J., Ribeiro, R. C. J., Wagner, R. L., Nguyen, H., Apriletti, J. W., Fletterick, R. J., Baxter, J. D., Kushner, R. J., and West, B. L. (1998) Hormone-dependent coactivator binding to a hydrophobic cleft on nuclear receptors, *Science 280*, 1747−1749.
10. Marimuthu, A., Feng, W. J., Tagami, T., Nguyen, H., Jameson, J. L., Fletterick, R. J., Baxter, J. D., and West, B. L. (2002) TR surface and conformations required to bind nuclear receptor correpressor, *Mol. Endocrinol. 16*, 271−286.
11. Ribeiro, R. C. J., Feng, W., Wagner, R. L., Costa, C. H. R. M., Pereira, A. C., Apriletti, J. W., Fletterick, R. J., and Baxter, J. D. (2001) Definition of the surface in the thyroid hormone receptor ligand binding domain for association as homodimers and heterodimers with retinoid X receptor, *J. Biol. Chem. 276*, 14987−14995.
12. Togashi, M., Nguyen, P., Fletterick, R., Baxter, J. D., and Webb, P. (2005) Rearrangements in thyroid hormone receptor charge clusters that stabilize bound 3,5′,5-triiodo-L-thyronine and inhibit homodimer formation, *J. Biol. Chem. 280*, 25665−25673.
13. Khorasanizadeh, S., and Rastinejad, F. (2001) Nuclear receptor interactions on DNA-response elements, *Trends Biochem. Sci. 26*, 384−390.
14. Weatherman, R. V., Fletterick, R. J., and Scanlan, T. S. (1999) Nuclear-receptor ligands and ligand-binding domains, *Annu. Rev. Biochem. 68*, 559−581.
15. Moras, D., and Gronemeyer, H. (1998) The nuclear receptor ligand-binding domain: Structure and function, *Curr. Opin. Cell Biol. 10*, 384−391.
16. Rastinejad, F., Perlmann, T., Evans, R. M., and Sigler, P. B. (1995) Structural determinants of nuclear receptor assembly on DNA direct repeats, *Nature 375*, 203−211.
17. Wagner, R. L., Huber, B. R., Shiau, A. K., Kelly, A., Lima, S. T. C., Scanlan, T. S., Apriletti, J. W., Baxter, J. D., West, B. L., and Fletterick, R. J. (2001) Hormone selectivity in thyroid hormone receptors, *Mol. Endocrinol. 15*, 398−410.
18. Nascimento, A. S., Dias, S. M. G., Nunes, F. M., Aparício, R., Ambrosio, A. L. B., Bleicher, L., Figueira, A. C. M., Santos, M. A. M., Neto, M. O., Fischer, H., Togashi, M., Craievich, A. F., Garratt, R. C., Baxter, J. D., Webb, P., and Polikarpov, I. (2006) Structural rearrangements in the thyroid hormone receptor hinge domain and their putative role in the receptor function, *J. Mol. Biol. 360*, 586−598.
19. Mengeling, B. J., Pan, F., and Privalsky, M. L. (2005) Novel mode of deoxyribonucleic acid recognition by thyroid hormone receptors: Thyroid hormone receptor β-isoforms can bind as trimers to natural response elements comprised of reiterated half-sites, *Mol. Endocrinol. 19*, 35−51.
20. Figueira, A. C. M., Dias, S. M. G., Apriletti, J. W., Baxter, J. D., Webb, P., Neves, F. A. R., Simeoni, L. A., Ribeiro, R. C. J., and Polikarpov, I. (2006) Human thyroid receptor forms tetramers in solution, which dissociate into dimers upon ligand binding, *Cell Biochem. Biophys. 44*, 453−462.
21. Kersten, S., Kelleher, D., Chambon, P., Gronemeyer, H., and Noy, N. (1995) Retinoid X receptor α forms tetramers in solution, *Proc. Natl. Acad. Sci. U.S.A. 92*, 8645−8649.
22. Kersten, S., Pan, L., Chambon, P., Gronemeyer, H., and Noy, N. (1995) Role of ligand in retinoid signaling. 9-cis-Retinoic acid modulates the oligomeric state of the retinoid X receptor, *Biochemistry 34*, 13717−13721.
23. Kersten, S., Pan, L., and Noy, N. (1995) On the role of ligand in retinoid signaling:Positive cooperativity in the interactions of 9-cis retinoic acid with tetramers of the retinoid X receptor, *Biochemistry 34*, 14263−14269.
24. Bourguet, W., Ruff, M., Chambon, P., Gronemeyer, H., and Moras, D. (1995) Crystal structure of the ligand-binding domain of the human nuclear receptor RXR-α, *Nature 375*, 377−382.
25. Nolte, R. T., Wisely, G. B., Westin, S., Cobb, J. E., Lambert, M. H., Kurokawa, R., Rosenfeld, M. G., Willson, T. M., Glass, C. K., and Milburn, M. V. (1998) Ligand binding and co-activator assembly of the peroxisome proliferator-activated receptor-gamma, *Nature 395*, 137−143.
26. Kallen, J., Schlaeppi, J. M., Bitsch, F., Filipuzzi, I., Schilb, A., Riou, V., Graham, A., Strauss, A., Geiser, M., and Fournier, B. (2004) Evidence for ligand-independent transcriptional activation of the human estrogen-related receptor α (ERRα): Crystal structure of ERRα ligand binding domain in complex with peroxisome proliferator-activated receptor coactivator-1α, *J. Biol. Chem. 279*, 49330−49337.
27. Sablin, E. P., Krylova, I. N., Fletterick, R. J., and Ingraham, H. A. (2003) Structural basis for ligand-independent activation of the orphan nuclear receptor LRH-1, *Mol. Cell 11*, 1575−1585.
28. Wang, Z., Benoit, G., Liu, J., Prasad, S., Arnisalo, P., Liu, X., Xu, H., Walker, N., and Perlmann, T. (2003) Structure and function of Nurr1 identifies a class of ligand-independent nuclear receptors, *Nature 423*, 555−560.
29. Greschik, H., Wurtz, J.-M., Sanglier, S., Bourguet, W., van Dorsselaer, A., Moras, D., and Renaud, J. P. (2002) Structural and functional evidence for ligand-independent transcriptional activation by the estrogen-related receptor 3, *Mol. Cell 9*, 303−313.
30. Fischer, H., Dias, S. M. G., Santos, M. A. M., Alves, A. C., Zanchin, N., Craievich, A. F., Apriletti, J. W., Baxter, J. D., Webb, P., Neves, F. A. R., Ribeiro, R. C. J., and Polikarpov, I. (2003) Low resolution structures of the retinoid X receptor DNA-binding and ligand-binding domains revealed by synchrotron X-ray solution scattering, *J. Biol. Chem. 278*, 16030−16038.
31. Khurana, R., Uversky, V. N., Nielsen, L., and Fink, A. L. (2001) Is Congo red an amyloid-specific dye? *J. Biol. Chem. 276*, 22715−22721.
32. de la Torre, J. G., Navarro, S., Lopez Martinez, M. C., Diaz, F. G., and Cascales, J. L. (1994) HYDRO: A computer program for the prediction of hydrodynamic properties of macromolecules, *Biophys. J. 67*, 530−531.
33. Kellermann, G., Vicentin, F., Tamura, E., Rocha, M., Tolentino, H., and Barbosa, A. (1997) The small-angle X-ray scattering beamline of the Brazilian synchrotron light laboratory, *J. Appl. Crystallogr. 30*, 880−883.
34. Svergun, D. I. (1992) Determination of the regularization parameter in indirect-transform methods using perceptual criteria, *J. Appl. Crystallogr. 25*, 495−503.
35. Glatter, O., and Kratky, O. (1982) *Small Angle X-ray Scattering*, Academic Press, London.
36. Svergun, D. I. (1999) Restoring low resolution structure of biological macromolecules from solution scattering using simulated annealing, *Biophys. J. 76*, 2879−2886.
37. Guinier, A., and Fournet, G. (1955) *Small-Angle Scattering of X-rays*, John Wiley, New York.
38. Svergun, D. I., Volkov, V. V., Kozin, M. B., and Stuhrmann, H. B. (1996) New developments in direct shape determination from small-angle scattering. 2, Uniqueness, *Acta Crystallogr. A52*, 419−426.
39. Svergun, D. I., Volkov, V. V., Kozin, M. B., Stuhrmann, H. B., Barberato, C., and Koch, M. H. (1997) Shape determination from solution scattering of biopolymers, *J. Appl. Crystallogr. 30*, 798−802.
40. Sturmann, H. B. (1970) New method for determination of surface form and internal structure of dissolved globular proteins from small angle X-ray measurements, *J. Chem. Phys. 72*, 177−182.
41. Shannon, C. E., and Weaver, W. (1949) *The Mathematical Theory of Communication*, University of Illinois Press, Urbana, IL.

42. Kersten, S., Reczek, P., and Noy, N. (1997) The tetramerization region of the retinoid X receptor is important for transcriptional activation by the receptor, *J. Biol. Chem. 272*, 29759−29768.
43. Kersten, S., Dong, D., Lee, W., Reczek, P., and Noy, N. (1998) Auto-silencing by the retinoid X receptor, *J. Mol. Biol. 284*, 21−32.
44. Chen, H., and Privalsky, M. L. (1995) Cooperative formation of high-order oligomers by retinoid X receptors: An unexpected mode of DNA recognition, *Proc. Natl. Acad. Sci. U.S.A. 92*, 422−426.
45. Lin, B. C., Wong, C. W., Chen, H. W., and Privalsky, M. L. (1997) Plasticity of tetramer formation by retinoid X receptors. An alternative paradigm for DNA recognition, *J. Biol. Chem. 272*, 9860−9867.
46. Bourguet, W., Vivat, V., Wurtz, J. M., Chambon, P., Gronemeyer, H., and Moras, D. (2000) Crystal structure of a heterodimeric complex of RAR and RXR ligand-binding domains, *Mol. Cell 5*, 289−298.
47. Gampe, R. T., Jr., Montana, V. G., Lambert, M. H., Wisely, G. B., Milburn, M. V., and Xu, H. E. (2000) Structural basis for autorepression of retinoid X receptor by tetramer formation and the AF-2 helix, *Genes Dev. 14*, 2229−2241.
48. de Groot, A., de Rosny, E., Juillan-Binard, C., Ferrer, J. L., Laudet, V., Pierce, R. J., Pebay-Peyroula, E., Fontecilla-Camps, J. C., and Borel, F. (2005) Crystal structure of a novel tetrameric complex of agonist-bound ligand-binding domain of *Biomphalaria glabrata* retinoid X receptor, *J. Mol. Biol. 354*, 841−853.
49. Tanenbaum, D. M., Wang, Y., Williams, S. P., and Sigler, P. B. (1998) Crystallographic comparison of the estrogen and progesterone receptor's ligand binding domains, *Proc. Natl. Acad. Sci. U.S.A. 95*, 5998−6003.
50. Egea, P. F., Rochel, N., Birck, C., Vachette, P., Timmins, P. A., and Moras, D. (2001) Effects of ligand binding on the association properties and conformation in solution of retinoic acid receptors RXR and RAR, *J. Mol. Biol. 307*, 557−576.
51. Kozin, M. B., and Svergun, D. I. (2001) Automated matching of high- and low-resolution structural models, *J. Appl. Crystallogr. 34*, 33−41.
52. Ye, L., Li, Y. L., Mellstrom, K., Mellin, C., Bladh, L. G., Koehler, K., Garg, N., Garcia Collazo, A. M., Litten, C., Husman, B., Persson, K., Ljunggren, J., Grover, G., Sleph, P. G., George, R., and Malm, J. (2003) Thyroid receptor ligands. 1. Agonist ligands selective for the thyroid receptor β1, *J. Med. Chem. 46*, 1580−1588.
53. Marti-Renom, M. A., Stuart, A., Fiser, A., Sánchez, R., Melo, F., and Sali, A. (2000) Comparative protein structure modeling of genes and genomes, *Annu. Rev. Biophys. Biomol. Struct. 29*, 291−325.
54. Collaborative Computational Project Number 4 (1994) *Acta Crystallogr. D50*, 760−763.
55. Emsley, P., and Cowtan, K. (2004) Coot: Model-building tools for molecular graphics, *Acta Crystallogr D60*, 2126−2132.
56. Konarev, P. V., Petoukhov, M. V., and Svergun, D. I. (2001) MASSHA: A graphics system for rigid-body modelling of macromolecular complexes against solution scattering data, *J. Appl. Crystallogr. 34*, 527−532.
57. Svergun, D. I., Barberato, C., and Koch, M. H. (1995) CRYSOL: A program to evaluate X-ray solution scattering of biological macromolecules from atomic coordinates, *J. Appl. Crystallogr. 28*, 768−773.
58. Yoh, S. M., and Privalsky, M. L. (2001) Transcriptional repression by thyroid hormone receptors: A role for receptor homodimers in the recruitment of SMRT corepressor, *J. Biol. Chem. 276*, 16857−16867.
59. Wu, Y., Xu, B., and Koenig, R. J. (2001) Thyroid hormone response element sequence and the recruitment of retinoid X receptors for thyroid hormone responsiveness, *J. Biol. Chem. 276*, 3929−3936.
60. Chen, Z. P., Iyer, J., Bougert, W., Held, P., Mioskowski, C., Lebeau, L., Noy, N., Chambon, P., and Gronemeyer, H. (1998) Ligand- and DNA-induced dissociation of RXR tetramers, *J. Mol. Biol. 275*, 55−65.
61. Kersten, S., Gronemeyer, H., and Noy, N. (1997) The DNA binding pattern of the retinoid X receptor is regulated by ligand-dependent modulation of its oligomeric state, *J. Biol. Chem. 272*, 12771−12777.
62. Peet, D. J., Doyle, D. F., Corey, D. R., and Mangelsdorf, D. J. (1998) Engineering novel specificities for ligand-activated transcription in the nuclear hormone receptor RXR, *Chem. Biol. 5*, 13−21.
63. Vivat, V., Zechel, C., Wurtz, J. M., Bourguet, W., Kagechika, H., Umemiya, H., Shudo, K., Moras, D., Gronemeyer, H., and Chambon, P. (1997) A mutation mimicking ligand-induced conformational change yields a constitutive RXR that senses allosteric effects in heterodimers, *EMBO J. 16*, 5697−5709.
64. Muscat, G. E., Griggs, R., Norman, M. F., Lavin, T. N., Baxter, J. D., and West, B. L. (1989) The rat growth hormone gene contains multiple thyroid response elements, *J. Biol. Chem. 264*, 12063−12073.
65. Muscat, G. E., Griggs, R., Downes, M., and Emery, J. (1993) Characterization of the thyroid hormone response element in the skeletal α-actin gene: Regulation of T3 receptor binding by retinoid X receptor, *Cell Growth Differ. 4*, 269−279.
66. Muscat, G. E., Mynett-Johnson, L., Dowhan, D., Downes, M., and Griggs, R. (1994) Activation of MyoD gene transcription by 3,5,3′-triiodo-L-thyronine: A direct role for thyroid hormone and retinoid X receptors, *Nucleic Acids Res. 22*, 583−591.
67. Massaad, C., Coumoul, X., Sabbah, M., Garlatti, M., Redeuilh, G., and Barouki, R. (1998) Properties of overlapping EREs: Synergistic activation of transcription and cooperative binding of ER, *Biochemistry 37*, 6023−6032.
68. Ponglikitmongkol, M., White, J. H., and Chambon, P. (1990) Synergistic activation of transcription by the human estrogen receptor bound to tandem responsive elements, *EMBO J. 9*, 2221−2231.
69. Garlatti, M., Daheshia, M., Slater, E., Bouguet, J., Hanoune, J., Beato, M., and Barouki, R. (1994) A functional glucocorticoid-responsive unit composed of two overlapping inactive receptor-binding sites: Evidence for formation of a receptor tetramer, *Mol. Cell. Biol. 14*, 8007−8017.

BI061698H